Tectonics®

RESEARCH ARTICLE
10.1029/2022TC007305

Ten Thousand Years of Paleo-Earthquakes Record of the Magallanes-Fagnano Plate Boundary Fault in Tierra del Fuego, Argentina

Sandrine Roy[1], Riccardo Vassallo[1], Joseph Martinod[1], and Christian Sue[1]

[1]ISTerre, CNRS, IRD, Université Grenoble Alpes, Université Savoie Mont Blanc, Université Gustave Eiffel, Le Bourget-du-Lac, France

Key Points:

- New records of at least six Holocene rupture events or phases in the eastern onshore portion of the Magallanes-Fagnano Fault
- During the last two millennia, three major rupture events dated in a paleoseismological trench at 1949 CE, 860 ± 130 and at 2160 ± 170 cal yrs BP
- The Magallanes-Fagnano Fault may break in "paired earthquakes" separated by less than 1 or 2 centuries

Supporting Information:

Supporting Information may be found in the online version of this article.

Correspondence to:

R. Vassallo,
riccardo.vassallo@univ-smb.fr

Citation:

Roy, S., Vassallo, R., Martinod, J., & Sue, C. (2023). Ten thousand years of paleo-earthquakes record of the Magallanes-Fagnano plate boundary fault in Tierra del Fuego, Argentina. *Tectonics*, *42*, e2022TC007305. https://doi.org/10.1029/2022TC007305

Received 15 MAR 2022
Accepted 30 MAR 2023

Author Contributions:

Conceptualization: Sandrine Roy, Riccardo Vassallo
Data curation: Sandrine Roy, Joseph Martinod
Formal analysis: Riccardo Vassallo, Joseph Martinod, Christian Sue
Funding acquisition: Riccardo Vassallo, Joseph Martinod, Christian Sue
Investigation: Sandrine Roy, Riccardo Vassallo, Joseph Martinod, Christian Sue
Methodology: Sandrine Roy, Riccardo Vassallo
Project Administration: Riccardo Vassallo

Abstract The Magallanes-Fagnano Fault is an active left-lateral strike-slip fault that cuts across Tierra del Fuego, forming the boundary between the South American and the Scotia plates. This fault may trigger strong earthquakes, as documented by the occurrence of two Mw ≥ 7.5 in December 1949. However, this region is characterized by one of the shortest historical archives in the world and by a growing population. The geological record is therefore needed in order to characterize the seismic information over a longer time scale and to improve the seismic hazard assessment. We conducted extensive field work, neotectonic mapping and excavated two paleoseismic trenches across one of the sharpest tectonic scarps in the Eastern onshore portion of the fault. Using scarp-derived colluvial wedges, cross-cutting relations, and 28 radiocarbon samples, we document evidences of at least six paleo-earthquakes during the Holocene. Paleoseismic record is particularly accurate for the last two thousand years, for which period we determine an average recurrence interval of 1080 ± 150 years. For repeated earthquakes of same magnitude as the 1949 event, this recurrence interval is compatible both with the known geodetic and geomorphic slip rates. However, "paired earthquakes" in less than one or two centuries may also occur, suggesting that fault behavior could be characterized by irregular seismic cycles.

Plain Language Summary The Magallanes-Fagnano Fault is a main active fault in Tierra del Fuego, at the southern tip of South America. This remote region has one of the shortest historical seismic record in the world. However, this fault may trigger strong earthquakes as occurred in 1949 and the surrounding population has been massively growing since. We therefore studied the paleo-earthquake history of the fault to improve the seismic hazard assessment. We analyzed and dated the disrupted sediments in two trenches excavated across the fault to establish a paleo-earthquake calendar. We document evidences of at least six paleo-earthquakes during the last ten thousand years. Paleoseismic record is particularly accurate for the last two thousand years, for which period we determine a recurrence interval of 1080 +/− 150 years. However, "paired" major earthquakes in less than one or two centuries may also occur, suggesting that fault behavior could not be based on regular seismic cycles.

1. Introduction

1.1. Tectonic Context

The Magallanes-Fagnano Fault (MFF) is a major left-lateral fault system that separates the austral segment of South America from the Scotia Plate (Ghiglione, 2002; Klepeis, 1994; Lodolo et al., 2003; Tassone et al., 2005, 2008; Torres-Carbonell et al., 2008; Winslow, 1982). This left-lateral plate boundary continues over almost 3,000 km, from the Pacific entrance of the Magellan Strait to the West, to the North Scotia Ridge and the Scotia subduction zone in the Atlantic Ocean to the East (Figure 1a). Most of this transform fault zone is offshore, Tierra del Fuego representing the largest onshore section of the fault system. The fault crosses the island on ∼180 km from the Almirantazgo Sound in Chile to the Atlantic Ocean in Argentina, but a large part of the fault is located beneath the 100 km-long Fagnano Lake (Figure 1b). In Argentina, the fault outcrops onshore on approximately 70 km between the eastern edge of the lake and the Atlantic coast (Figure 1c).

Although the analysis of brittle deformation and clastic dikes orientations suggest that some left-lateral strike-slip motion may have been accommodated along the fault zone since the Oligocene or early Miocene (Ghiglione, 2002; Ghiglione & Ramos, 2005; Klepeis, 1994), it appears that the onset of strike-slip faulting in Tierra del Fuego

Resources: Sandrine Roy, Joseph Martinod, Christian Sue
Software: Sandrine Roy
Supervision: Riccardo Vassallo, Joseph Martinod
Validation: Riccardo Vassallo, Joseph Martinod
Visualization: Riccardo Vassallo, Joseph Martinod
Writing – original draft: Sandrine Roy
Writing – review & editing: Riccardo Vassallo, Joseph Martinod, Christian Sue

along the MFF mainly occurred during the late Miocene (Torres-Carbonell et al., 2014). This tectonic phase followed the end of shortening in the Fuegian fold and thrust belt and the shift of activity from the East Scotia to the West Scotia spreading Ridge (Eagles & Jokat, 2014). The total amount of strike-slip motion accommodated by the fault has been estimated, considering pre-existing thrust faults displaced by the MFF, to 48 km in Argentina (Torres-Carbonell et al., 2008), and to 25 km in Chile (Klepeis, 1994) but a precise determination of this value is difficult because pre-existing compressive structures present a small obliquity with respect to the MFF azimuth. Tectonic data indicate that the motion accommodated by the fault system since the late Miocene has essentially been transcurrent with only a minor vertical component.

Lodolo et al. (2003) describe the MFF geometry and show that several *en echelon* pull-apart basins developed along the MFF, both in the Atlantic Ocean and Magallanes Strait. They also consider that the Fagnano Lake depression, although it has been carved by glacial erosion, corresponds to a major asymmetric transtensional structure. Esteban et al. (2014) analyzed bathymetric and seismic data available in the lake and confirm that it is composed of 4 amalgamated pull-apart sub-basins. In contrast, between the eastern edge of Lago Fagnano and the Atlantic coast, there is no evidence of major active pull-apart basin except perhaps the very small Udaeta Lake pull-apart (Onorato et al., 2017). Roy et al. (2020) and Onorato et al. (2021) mapped this region of the fault. They divide the fault in several sections presenting a particular geomorphological expression, but the fault is everywhere essentially transcurrent. Reiteration of geodetic networks in the Argentinean sector of Tierra del Fuego evidences that the MFF is now accommodating 5.9 ± 0.2 mm/yr of sinistral strike-slip motion between the Scotia plate and South America (Mendoza et al., 2015; Smalley et al., 2003), without significant transtension or transpression. This is also the average Late Pleistocene - Holocene rate estimated considering post-glacial markers offsets (Roy et al., 2020; Sandoval & De Pascale, 2020). Actually, considering that this velocity remained constant since the Late Miocene reorganization of the Scotia Plate and the appearance of the West Scotia Ridge, this motion would explain the long-term observed offset of pre-existing structures by the fault (Torres-Carbonell et al., 2014). Geomorphological observations evidence that depending on the section considered between the eastern shore of the Fagnano Lake and the Atlantic Coast, either the northern or the southern block are affected by a small relative uplift. However, the cumulated relative uplift registered by post-glacial landforms rarely exceeds 10 m, meanwhile the horizontal offset during the same period interval was around 110–130 m (Roy et al., 2020; Sandoval & De Pascale, 2020), confirming that the dip slip component accommodated by the MFF in the area located between the eastern end of the Fagnano Lake and the Atlantic Coast is modest compared to the strike-slip displacement.

1.2. Historical Seismicity

Several major earthquakes ($M \geq 7$) occurred along the MFF during the last century and their focal mechanisms confirm sinistral strike-slip motion along the fault (Figure 1b). Onshore in Tierra del Fuego, the largest events occurred in 1949 on the same day: on December 17, a first shock of magnitude Mw 7.75 occurred at 6:53 (GMT), and another of magnitude Mw 7.5 at 15:07 (GMT) struck off, followed by several aftershocks of unknown magnitude (Febrer et al., 2000; Jaschek et al., 1982; Pelayo & Wiens, 1989). Those shocks were widely felt across the entire Tierra del Fuego archipelago, in the Magallanes (Chile) and Santa Cruz (Argentina) Provinces (INPRES, 2021; Isla & Bujalesky, 2004; Lomnitz, 1970; Perucca et al., 2016). One hundred and forty nine epicenters are located in the region of the Karukinka natural park, ~50 km north of the MFF, but are affected by substantial uncertainties (Figure 1b) (Adaros et al., 1999; Febrer et al., 2000; Jaschek et al., 1982). Observed surface ruptures confirm that these earthquakes activated the main branch of the fault (Costa et al., 2006; Onorato et al., 2021; Roy et al., 2020). Roy et al. (2020) report evidence of surface ruptures with up to 6.5 m of sinistral lateral offset along the MFF in the Argentinean sector of Tierra del Fuego, between the Lago Fagnano and the Atlantic Ocean. Fresh surface ruptures have also been reported by Roy (2020) along the Chilean portion of the fault for a total length of more than 150 km, which is coherent with the known magnitude of the 1949 earthquakes.

Historical information is particularly short in Tierra del Fuego, since the first European person established permanently in the island only in 1868 (Rev. Thomas Bridges). It explains why earthquakes that occurred during the 19th century are at best poorly known, and why no historical catalogs exist before 1868. In 1879, 1 February, several inhabitants and navigators reported a succession of shocks of great intensity (Bridges & Canclini, 2001; Brüggen, 1943; Bustos, 1931; Cisternas & Vera, 2008; Dublé Almeida, 1938; Martinic, 1988; Montessus de Ballore, 1912; Palacios, 2013; Serrano, 1880; Simpson & Chaigneau, 1880). Based on these

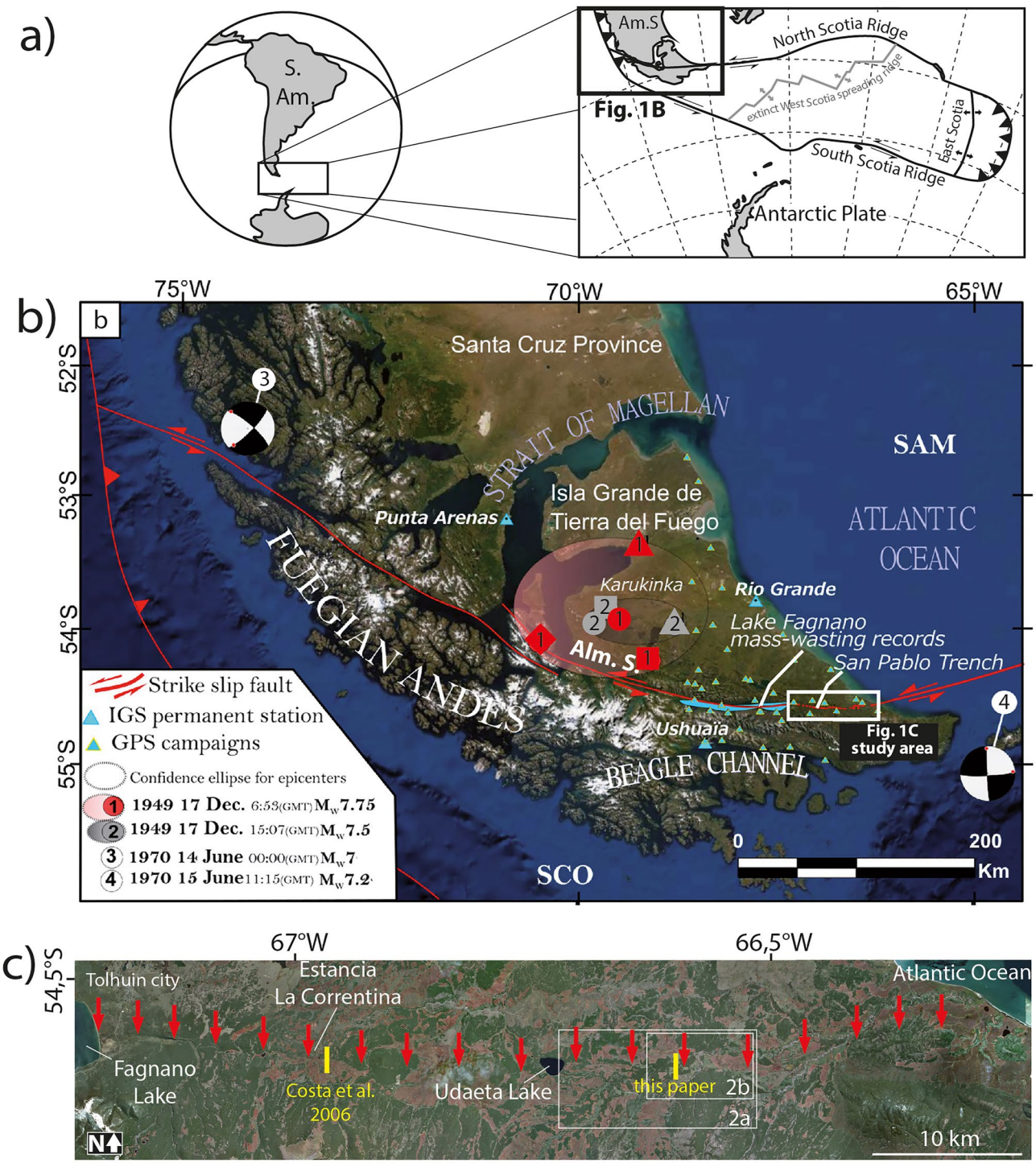

Figure 1. (a) Geodynamic setting of the study area. (b) Regional tectonic setting. Epicenters of $M \geq 7$ earthquakes and focal mechanisms, when available, according to U.S. Geological Survey (2021) (circles), Castano (1977) (diamond), Jaschek et al. (1982) (squares), Pelayo and Wiens (1989) (triangles). In this figure are located also the GNSS network occupied by Mendoza et al. (2015) in the Argentinean sector of Tierra del Fuego, the San Pablo paleoseismic trench (Costa et al., 2006) and the Lago Fagnano where mass wasting events were studied by Waldmann et al. (2011). SAM = South American Plate; SCO = Scotia Plate; Alm. S. = Almirantazgo Sound. (c) Red arrows point at the trace of the main MFF that ruptured in 1949 onshore (Roy et al., 2020) in the Argentinean Tierra del Fuego (Google Earth images). Yellow rectangles are the trench sites from Costa et al. (2006) and this work.

observations, an intensity of VII and possibly VIII on the Modified Mercalli scale was estimated in Tierra del Fuego (Lomnitz, 1970). This author proposes that the magnitude of the 1879 earthquake was 7–7.5. To date, there is no reliable location, but the collected testimonies define a broad impacted zone from 50° to 54.5°S (Martinic, 2008).

The native hunter-gatherer groups probably underwent several earthquakes since their southward migration in the Fuegian archipelago at the end of Pleistocene, from 13 to 10.5 ka BP (Massone, 2004; Miotti & Salemme, 2004; Salemme & Miotti, 2008). A reference to a prehistoric event originated from a Yagán tale is mentioned by E.L. Bridges, son of Thomas Bridges: *« A long time ago the moon fell into the sea, […] it rose in great tumult, just as the water rises from a bucket when a great stone falls inside. The only survivors of the flood were the fortunate inhabitants of Isla Gable […]. The surrounding mountains soon submerged, and the people […], looking around, saw nothing but the ocean to the edge of the horizon […]. »* (Bridges, 1948).

1.3. Paleoseismicity

Paleoseismic investigation allows analysis of a more extended history of major earthquakes with respect to the historical record (e.g., Wallace, 1981). Surface faulting geometries and disrupted stratigraphy constitute primary evidences for recognizing records of pre-historic paleo-earthquakes (McCalpin & Nelson, 1996; Obermeier, 1996; Sieh, 1981). Historical and instrumental records in Tierra del Fuego (52°S) are particularly scarce, because of this paleoseismological investigations are particularly critical to reconstruct the seismic history of this region.

Tierra del Fuego has been largely affected by Quaternary glaciations, which results in excellent opportunities for paleoseismic investigations. Indeed, the MFF disrupts Pleistocene to Holocene morphologies and superficial deposits that resulted from glacial and post-glacial processes (Costa et al., 2006; Lodolo et al., 2003; Onorato, 2018; Onorato et al., 2021; Roy et al., 2020; Sandoval & De Pascale, 2020; Waldmann et al., 2011; Winslow, 1982). Nevertheless, few studies of paleoseismicity have been published yet along the MFF. Costa et al. (2006) describe a trench realized across a secondary fault trace in the Argentinean sector of Tierra del Fuego, close to Rio San Pablo (see Figures 1b and 1c for location). They show evidence for three (possibly four) paleo-earthquakes that occurred during the last 8 ka, suggesting a maximum average recurrence interval between 2 and 3 ka. On the other hand, Waldmann et al. (2011) use the Lago Fagnano sediment archives to evidence mass-wasting events that may have resulted from paleo-earthquakes on faults nearby. They recognize 19 mass-wasting events over the last 11 ka and propose an average seismic recurrence interval varying between 350 and 850 years along the MFF (Figure 1b). In this contribution, we present results from two new paleoseismic trenches realized across the fault, evidencing at least six paleo-earthquakes. We integrate these new data within a reviewed chronology of paleo-earthquakes in Tierra del Fuego and discuss earthquakes magnitudes and recurrence along the MFF, considering the Late Pleistocene-Holocene fault slip rate.

2. Methods

We mapped the fault scarps related to the MFF using Pléiades satellite images, aerial photographs from unmanned aerial vehicle (UAV), trench site high-resolution-DEM, and cross-checked these observations in the field.

The trenches were gridded into 1 × 1-m squares. We pinpointed remarkable units and charcoals with flags to enable detailed and scale logging of structures, fault terminations and stratigraphy. Each sample has been selected in recognized units and originates from a single charcoal.

Radiocarbon measurements were made at the « Laboratoire de Mesures du Carbone 14 » (CEA Saclay, France). The ages are calibrated using Oxcal version 4.3 (Ramsey, 2009, 2017) with southern hemisphere calibrating curve SHCAL13 (Hogg et al., 2013). The raw ^{14}C ages (yrs BP) and the calibrated ages (cal yrs BP) are available in Table 1, and registered online with the International Geo Sample Numbers (IGSN) at System for Earth Sample Registration (SESAR, http://geosamples.org).

The paleoseismic analyses are based on field log, macro photographs and high-resolution orthophoto mosaics of the trench walls. As far as possible, the ages of the paleo-earthquakes are bracketed from the radiocarbon ages of units directly affected by ruptures or sealing them. However, in a context where unconsolidated deposits lying on the scarp slope are often eroded and information is lost for most of rupture terminations, these conditions are rarely realized. We therefore analyze the ruptures geometry, the stratigraphy and the spatial distribution of dated

Table 1
Mass Spectrometry Measurements of Radiocarbon Samples

N°	IGSN	mg C	Delta C13	pMC	Err pMC	Raw age (yrs BP)	Err (yrs)	Calibrated From	Age yrs BP To	Unit
C1	IEROY0001	1.42	−31.30	88.33	0.24	**995**	30	**964**	**798**	a
C2	IEROY0002	1.26	−29.00	68.35	0.21	**3055**	30	**3356**	**3180**	a
C3	IEROY0003	1.07	−28.1	30.88	0.16	**9440**	40	**10776**	**10565**	g
C4	IEROY0004	1.71	−28.7	88.15	0.22	**1015**	30	**979**	**802**	a
C5	IEROY0005	1.55	−24.8	75.99	0.21	**2205**	30	**2319**	**2145**	c
C6	IEROY0006	1.67	−29.1	76.71	0.21	**2130**	30	**2299**	**2001**	c
C7	IEROY0007	1.41	−24.9	75.97	0.21	**2205**	30	**2319**	**2145**	d
C8	IEROY0008	1.56	−22.7	76.5	0.22	**2150**	30	**2305**	**2010**	d
C9	IEROY0009	1.32	−30.4	76.88	0.22	**2110**	30	**2153**	**1995**	c
C10	IEROY000A	1.51	−28.8	77.01	0.22	**2100**	30	**2147**	**1996**	b*
C11	IEROY000B	1.41	−23.9	76.83	0.21	**2120**	30	**2294**	**1999**	b*
C12	IEROY000C	1.34	−27.3	75.96	0.21	**2210**	30	**2320**	**2148**	b*
C13	IEROY000D	1.38	−26.8	76.74	0.22	**2125**	30	**2297**	**2001**	b*
C14	IEROY000E	0.63	−31.9	76.56	0.22	**2145**	30	**2304**	**2007**	c
C15	IEROY000F	1.53	−23.7	89.53	0.23	**890**	30	**910**	**733**	a
C16		0.96	−26.8	106.48	0.25	Date out of range				c
C17	IEROY000G	0.29	−20.2	34.54	0.21	**8540**	50	**9595**	**9460**	f
C18	IEROY000H	0.38	−30.6	78.41	0.22	**1955**	30	**1987**	**1827**	a
C21	IEROY000I	0.33	−28.5	31.89	0.17	**9180**	45	**10490**	**10240**	g
C22	IEROY000J	0.84	−28.1	31.98	0.16	**9160**	40	**10478**	**10233**	g
C23	IEROY000K	0.18	−20.9	36.63	0.24	**8070**	50	**9130**	**8768**	g
C24	IEROY000L	0.13	−22.9	45.21	0.29	**6380**	50	**7424**	**7180**	g
C25	IEROY000M	1.47	−27	76.25	0.21	**2180**	30	**2310**	**2117**	c
C26	IEROY000N	1.32	−26	76.67	0.22	**2135**	30	**2300**	**2004**	b*
C27	IEROY000O	1.34	−20.3	76.63	0.22	**2140**	30	**2302**	**2006**	b*
C28	IEROY000P	1.62	−21	76.33	0.21	**2170**	30	**2309**	**2065**	b*
C29	IEROY000Q	1.26	−23.1	76.57	0.21	**2145**	30	**2304**	**2007**	b*
C30	IEROY000R	0.88	−29.7	75.82	0.22	**2225**	30	**2329**	**2152**	b*
C31	IEROY000S	1.39	−22.3	76.67	0.21	**2135**	30	**2300**	**2004**	b*

Note. Measurements done at LMC14, CEA Saclay, France. Calibrated ages are reported in cal yrs BP. Calibration done using the Oxcal version 4.3 (Ramsey, 2009) using atmospheric curve SHCal13 (Hogg et al., 2013). N° is lab number (IGSN International Geo Sample Numbers); mg C: amount of carbon in mg; pMC: percent Modern Carbon. Raw ages are available in the SESAR data repository (Roy et al., 2022). Bold values indicate raw and Cal BP sample ages.

coals to bracket the rupture ages. This analysis allows the building of palinspastic restorations, based on balanced cross-section principles (Elliott, 1983), as suggested by Mc Calpin (1996). These restorations are based on an interactive process to check the consistency between the initial and final stages of the cross-section. Such models are not meant to be unique, but the constraints given by the units' geometry/sedimentology and by the geochronological data minimize the plausible solutions. Finally, to correlate the latest ruptures with surface faults microtopography we use the DEM and the orthophoto mosaics of the trench walls (both built with Agisoft Metashape ©).

3. Study Site

The MFF outcrops for approximately 180 km on the island of Tierra del Fuego, half of which are beneath the Lago Fagnano. Roy et al. (2020) and Onorato et al. (2021) mapped the 70 km of the fault between the eastern edge

of Lago Fagnano and the Atlantic coast and showed that most of this portion broke during the 1949 earthquakes. They divided the fault in several sections on the basis of their geomorphological expression. The central zone of this part of the MFF, from west to east, is constituted by the Udaeta, the La Blanca and the Pop-up sections (Roy et al., 2020). While all these sections are characterized by dominant strike-slip kinematics, they can be associated with decameter to hectometer-scale structures reflecting local transtension (Udaeta section) or transpression (Pop-up section). Tectonic deformation along these two sections is often distributed over a relatively wide (up to 1 km) fault zone.

In the La Blanca fault section, most of the deformation is accommodated along a single surface rupture exposing remarkably continuous fault morphologies (Figure 2). The cumulated left-lateral movement, combined with a minor vertical component, uplifted the southern block relative to the northern block of the fault. This movement built a continuous scarp whose north-facing slope presents a steepness of ~20–30° (Figures 2–4). The scarp trends approximately E-W, and its height varies along strike from 1 up to 11 m. This fault section has been activated during the 1949 earthquakes, as evidenced by fences offset along the fault (Figure 2, Roy et al., 2020). The 1949 measured left-lateral horizontal co-seismic slip varies between 4.3 and 6.5 m in this area. In regard to this tectonic setting, the configuration favors a possible long record of faulting in the subsurface, making this fault section particularly relevant to paleoseismic investigations.

The morphology of the scarp is perturbed by scarplets of few tens centimeters high that are well-preserved in the topography. Among them, the surface shows *en-échelon* Riedel fractures corresponding to R-shear synthetic faults striking approximately N75°E (Figure 3). Superficial morphology including the presence of numerous Riedel structures along the fault is clearly visible in many other sectors of the MFF, such as the Pop-up section or close to the Estancia La Correntina (Roy et al., 2020) (Figure 1c). At the study site, four of these fractures cross our paleoseismological trenches.

We excavated two trenches across the fault (54.5591°S; 66.6211°W), about 5 km east of Lake Udaeta (Figure 2), in a flat area covered by post-glacial fluvial deposits that corresponds to an alluvial terrace of the Irigoyen River. At the trench site a north-facing, E-W cumulative scarp of 8–10 m high, separates the flat northern and southern blocks (Figures 3 and 4). This scarp is the result of the long-term vertical component of the fault section, associated with a 110–130 horizontal cumulative displacement (Roy et al., 2020). No active developed drainage system is visible in this flat area, with the exception of a very smooth relative depression in the higher southern block (up to one-m-deep over a 30-m-wide zone, see Figure 4b). Here, short-lived water flow resulted in regressive erosion that incised the southern block for up to 15 m and formed a local alluvial fan at the toes of the scarp. This incision created a natural outcrop across the fault zone where we established one of the trenches (Trench n°2, see Figures 3 and 4).

Trench n°1 was excavated from the mid to the base of the scarp, 20 m west of Trench n°2. It is 9-m long and 1.50 m deep. The trench pattern is a single downslope slot with an additional 80-cm wide westward enlargement along 3-m. Our paleoseismic reconstruction is based on the logging and dating of the two walls of this trench (Figures 5–9).

Trench n°2 is 13-m long and 4.5-m deep. In this second trench, we observed a single rupture crossing the scarp (fault A, Figures 3 and 4). Here, the location of the rupture toward the northern tip of the trench did not allow to observe a clear earthquakes-related stratigraphy nor datable organic matter. Therefore, we did not use this trench to establish a paleo-earthquakes chronology. However, this trench was useful in confirming the localization of significant tectonic deformation in a narrow part of the scarp. We therefore did not analyze this trench in detail. In the following, our observations, logging and dating refer only to Trench n°1.

4. Paleoseismological Results

4.1. Stratigraphy: Description of Units

The scarp comprises alluvial deposits associated with the terrace morphology, particularly visible in the natural incision where Trench n°2 is excavated, and colluvial deposits issued from the degradation of the slope due to tectonic and gravitational processes. We identified 12 units in Trench n°1. Units are labeled from the youngest unit a to the oldest unit j (Figure 5). A gray modern soil horizon labeled “s” caps the whole trench. The oldest exposed units j and i have the same alluvial imprint but show different structures. Unit j indicates the aggradation of river channels with a cross-bedded stratigraphy. Its coarse clasts size and the rounded cobbles highlight the

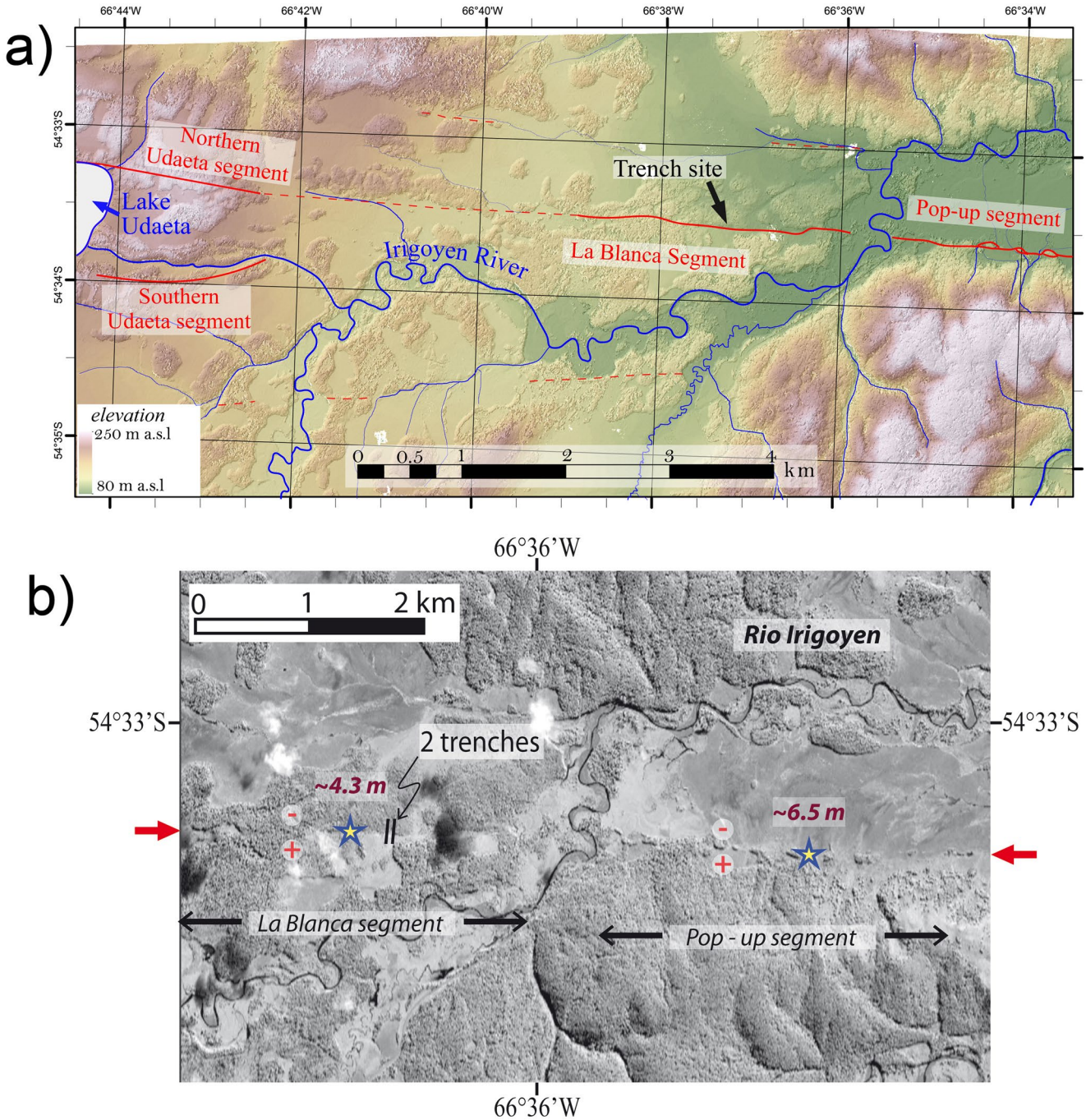

Figure 2. (a) Fault map of the study area on a Digital Elevation Model generated from 2018 Pleiades images (see Figures 1b and 1c for location). The red lines locate the fault scarps with cross-checked evidence of faulting in Pleistocene to Holocene surficial deposits, and the red dashed lines shows inferred fault traces, after Onorato (2018), Onorato et al. (2021), Roy et al. (2020), and Torres-Carbonell et al. (2008). (b) Pleiade image of the trench site area. The red +/− signs pinpoint the relative elevation changes between the blocks. The yellow stars indicate the location of fences offset by the 1949 earthquakes, with the reported left-lateral slip (Roy et al., 2020). The location of the two paleoseismological trenches is indicated by black lines.

high-energy and long-distance transportation. This unit constitutes the top of the terrace on the southern block. Unit i, though characterized by similar sedimentary composition, shows verticalized and fractured cobbles along the fault planes indicating localized tectonic reworking of the pristine alluvial material. These units are unconformably covered by units h and g, poorly sorted and without any bedding, which are the oldest colluvial deposits in the trench.

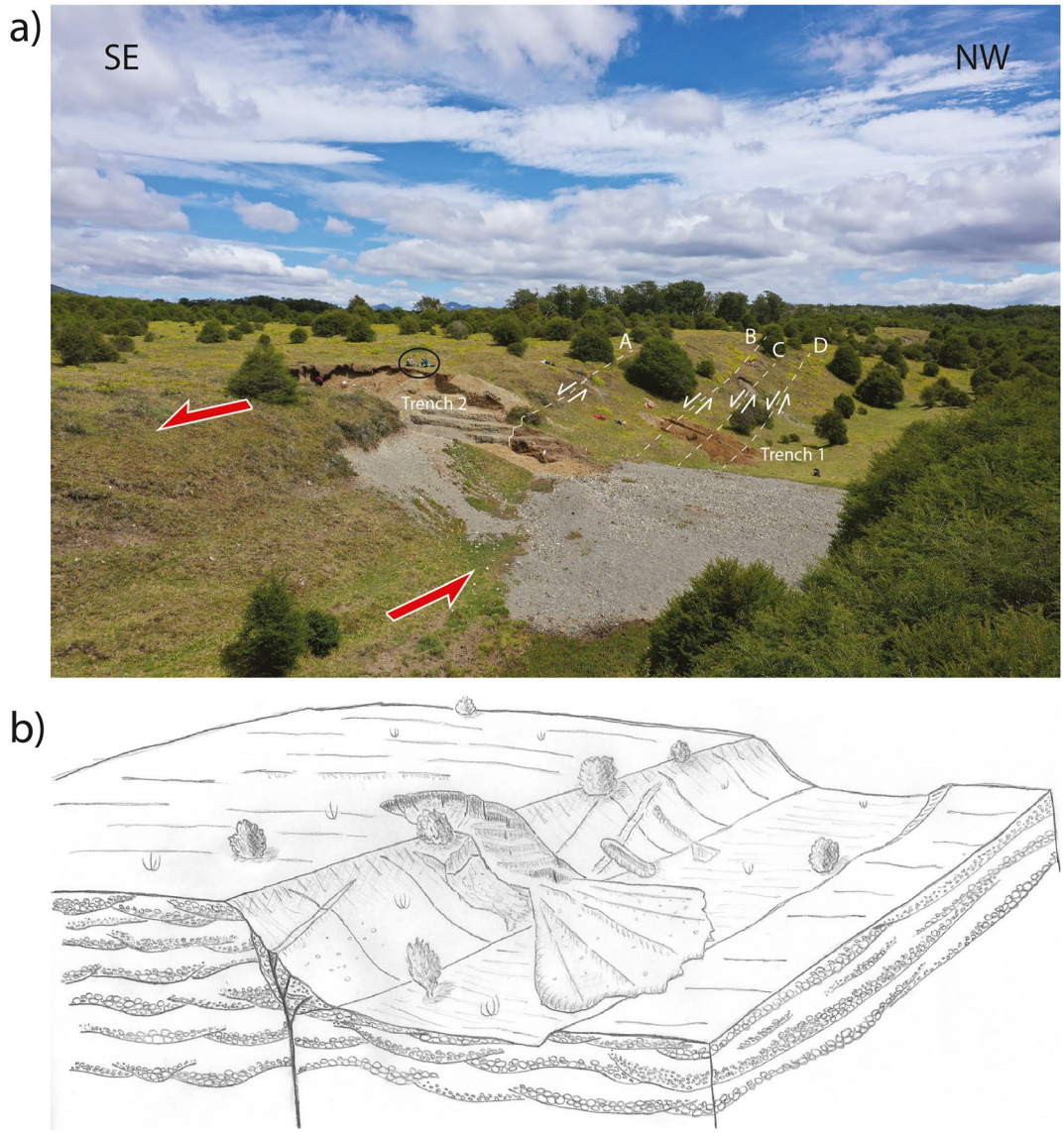

Figure 3. (a) Oblique view of the fault scarp (photo looks toward the SW). Trench n°2 reshapes a natural incision resulting from water flow from the southern uplifted block to the north. Trench n°1 is located ~20 m West of Trench n°2. Both trenches cut Riedel fractures oblique to the main fault scarp. Riedel fractures, labeled A to D, are visible in the morphology of the scarp. Red arrows indicate the main left-lateral kinematics of the fault zone. People in the black circle give the scale. (b) Block diagram showing the relationship between morpho-stratigraphy and tectonic structures observed within the trenches.

The overlying units f and e are much thinner (<20 cm) and rich in silt compared to the other units. These thicknesses and compositions may be related to loess accumulation that occurred in Tierra del Fuego during the Holocene (Coronato et al., 2011). Unit e shows a general oxidation state, likely due to weathering. It suggests a long period of exposure of this unit at the ground surface, without burying nor significant denudation.

Units d to b show bad sorting and lack of depositional structures. Their thickness is quite variable, between few cm and ~50 cm, thickening at the toes of the scarp. These characteristics suggests a gravitational transport, with remobilization of heterogeneous material along the slope. As unit h and g they may be defined as colluvial deposits.

Unit b* is thin, concave-shaped and is particularly rich in large charcoals. All these elements suggest the presence of an anthropic fire-place.

Unit a fills an open crack that cuts all other units. This unit is composed of dark silty-clay material at the top and gravels in a sandy matrix at the bottom, without sharp discontinuity between these two parts. No sorting is

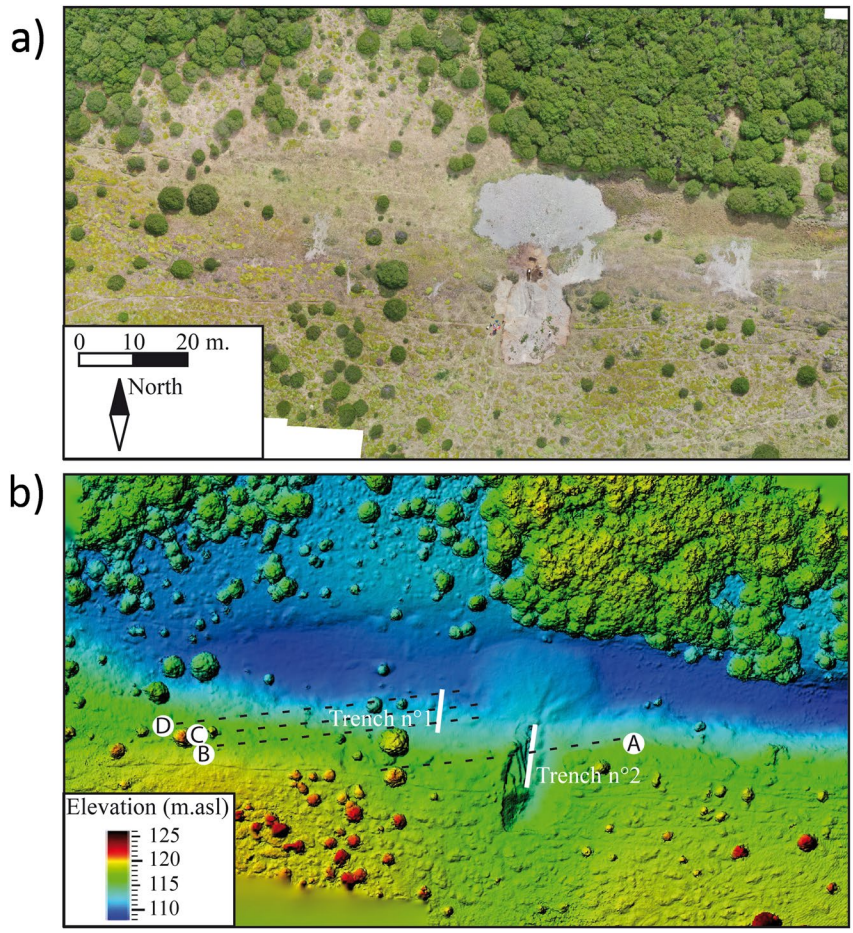

Figure 4. (a) Orthometric photography from Unmanned Aerial Vehicle (UAV) and (b) Digital Elevation Model (DEM) of the study area. Both were realized before Trench n°1 was dug.

observed. This is consistent with a relatively rapid filling of the fissure by loose material coming from the surface and from proximal units.

4.2. Sedimentary Units Dating

We dated 29 charcoals contained in six different sedimentary units using radiocarbon method. Analytical results are presented in Table 1 and samples position is reported on the trench logs (Figures 6 and 7). At total, only four samples out of 29 were considered as outliers because of their incompatibility with stratigraphic order and discarded for units dating.

Unit g is the oldest deposit where we found charcoals. Three samples yield quasi-identical ages range from 10,776 to 10,233 cal yrs BP. Two other samples are younger, but their age is not compatible with the age of the overlying unit f. They are also the two smaller samples of the whole set (<0.20 mg of carbon) and may be more sensitive to contamination with other organic matter during sampling. Given the relative consistency of the three older charcoals, we chose to attribute an age of 10776–10233 cal yrs BP to unit g.

Unit f contains one charcoal dated at 9595–9460 cal BP, consistent with the relative stratigraphic order and significantly younger than the age interval of unit g. Even if constrained by a single sample, we thus assume this age for unit f.

Dating of units d, c, b* is strongly constrained by 17 coherent samples. All samples are comprised between 2329–2152 (C30) and 2153–1995 (C9) cal yrs BP, with very little scattering. These units deposited several thousand years after unit f, and probably unit e, in a short period of few tens or hundreds of years. Since the

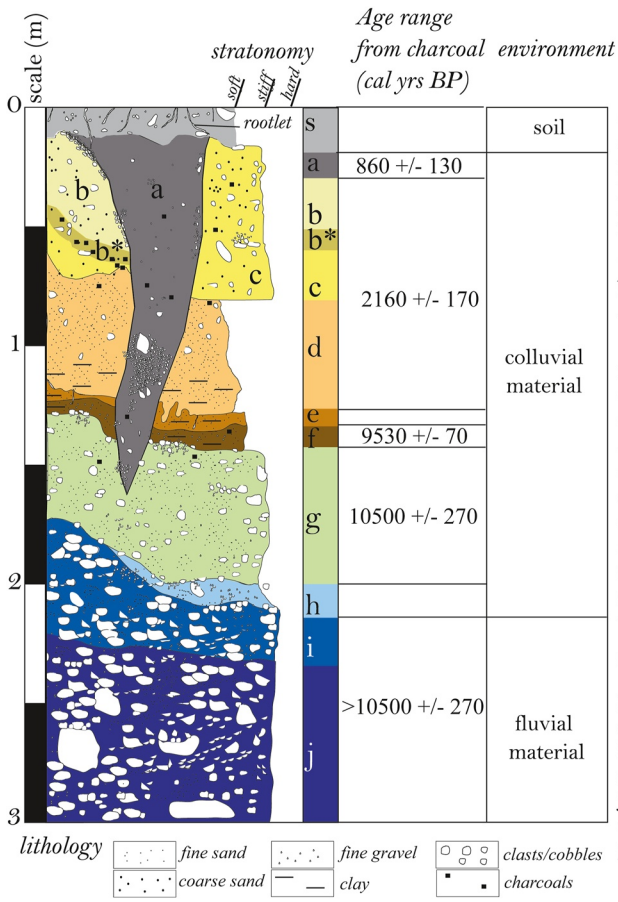

Description of units

s : greyish modern soil, with rootlets and medium to coarse pebbles .

a : grey filling of an open-crack (from tectonic activity) matrix-supported of fine-medium sand, clast-rich, strongly normal graded bedding of rounded gravel against lateral faults, and bottom of fissure, rare sub-angular cobble. Unit composed of reworked material from proximal units.

b : grey-compacted matrix-supported of fine sand, clast-rich, well-rounded, unsorted, coarse gravels.

b*: grey-black concave matrix-supported of fine-medium sand, 5-10 cm thick, charcoal-riched, origin ambiguous : roots, natural or anthropogenic fire?

c : brown-grey compacted matrix supported of fine light brown sand, rich in rounded unsorted coarse gravel, rarely downslope imbricated, rare rounded cobble (5-8cm).

d (upper): light brown unconsolidated matrix-supported of fine sand layer, some subrounded sorted coarse gravel.

d (lower): light brown unconsolidated matrix-supported of fine clayish-silt with fine medium sands, stiffness laterally variable.

e : orange (iron oxides) convolutes and folded shapes (liquefaction) of matrix supported stiff silty-clay, minor fine sand, rare rootlets, thickness laterally variable, rare medium pebble pockets injected in and above the unit.

f : dark brown matrix-supported of silty-clay, with rare gravel, thickness laterally variable.

g : brown-light grey clast-supported medium to coarse rounded gravels (no graded bedding), minor hard fine sandy matrix, lenticulars pocket of gravel and silty-sand.

h : clast-supported, minor sandy matrix, poorly sorted, no graded bedding, some re-oriented cobbles along faults.

i : same composition as unit j; Clast-supported, with tectonized structures: re-oriented cobbles along faults, fractured cobbles.

j : compact clast-supported, abundant organized cobble-pebble, large cross-bedded stratification, normal gradded bedding; Lenticular medium pebble pockets, imbricated pebbles with flow direction toward the E and NE; Slightly gravelly and sandy.

Figure 5. Synthetic sedimentary log, type of depositional environment, and description of units in Trench 1. We used the modified Udden–Wentworth grain-size scale (Blair & McPherson, 1999).

oldest and youngest samples of these units are indistinguishable in terms of age probability, an age range of 2329–1995 cal yrs BP applies to these three units.

Unit a contains three samples of similar age and two older ones. The open-crack is therefore filled with coeval and older remobilized material. This age distribution suggests fissure filling at 860 ± 130 cal yrs BP.

4.3. Recognition and Dating of Paleo-Earthquakes

Disrupted structures are exposed on both walls of Trench n°1. Most of the faults are paired with their equivalent geometry and kinematics on the opposite wall. The two walls of this trench exposed 20 faults truncating partially or entirely the section. They are grouped and interpreted in 6 rupture events or phases (Figures 8 and 9). Rupture events are well-constrained in time and are constituted by 1 paleo-earthquake or 2 paleo-earthquakes separated by a short time interval, while rupture phases cover a larger period of time and may be the result of several paleo-earthquakes.

Faults F9 and F12 affect alluvial units j and i. These ruptures and units are truncated by an erosion surface, partially covered by the oldest colluvial unit h. Their geometry and relative stratigraphy are compatible with the occurrence of a rupture phase, with an apparent normal kinematics, older than all the dated units in the trench. Rupture phase R1 is therefore older than ~10500 cal BP.

Faults F8, F10, F11, F13, and F16 also affect units j and i, putting in contact these alluvial units with colluvial units h (F10–F11) and g (F8, F13, F16). Because of this configuration and of the normal apparent offsets along the faults, we considered units h and g as colluvial wedges associated with a new rupture phase. Due to the impossibility of direct correlation between units h and g, this rupture phase may be related to one or more

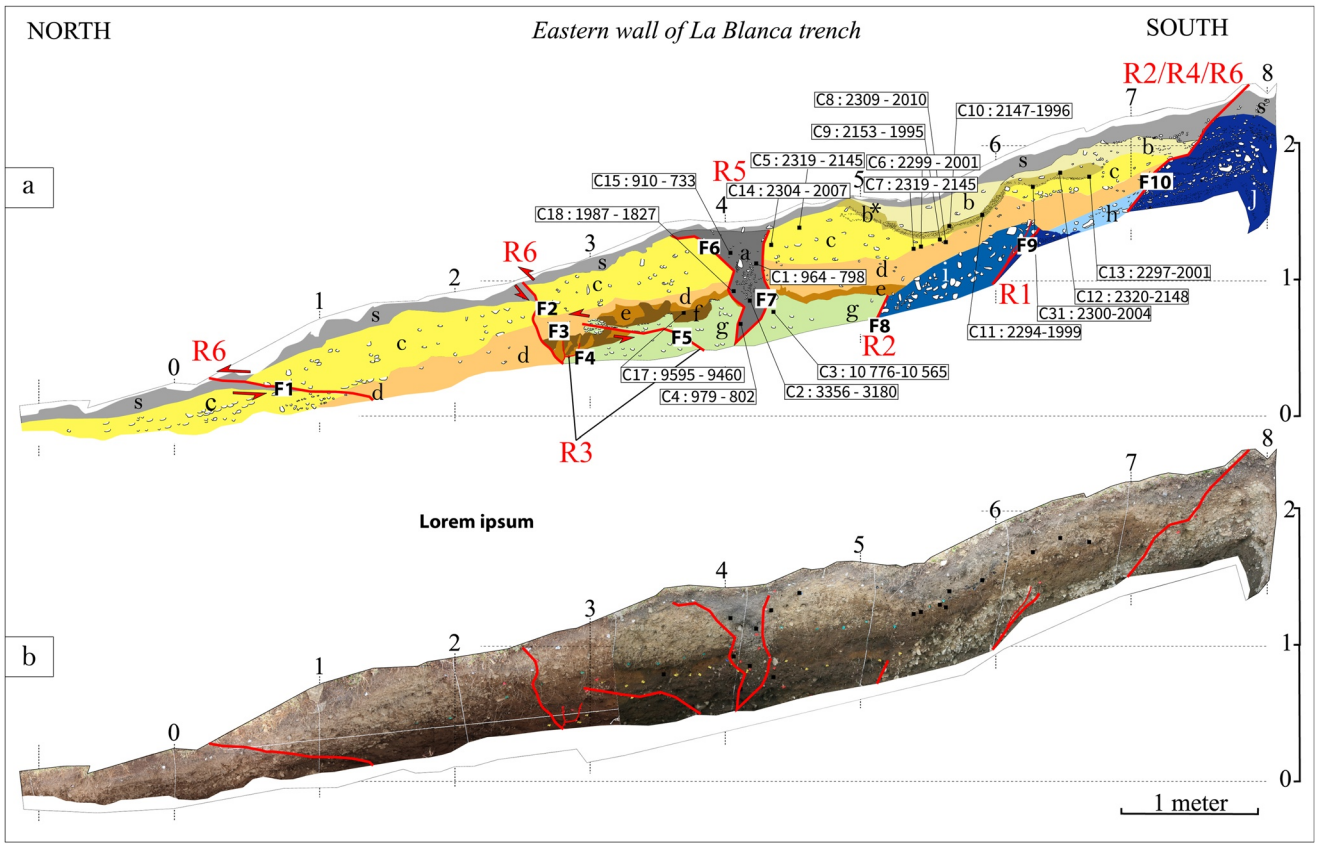

Figure 6. (a) Interpretation and (b) orthophoto mosaic of the eastern wall of Trench n°1. Small black squares show the locations of radiocarbon samples, labeled by sample numbers and their corresponding calibrated radiocarbon ages (cal yrs BP). Rupture events or phases (R), associated faults (F) and fault kinematics (arrows) are marked in red. Zoom on soft sediment deformation is available in Supporting Information S1.

paleo-earthquakes. Colluvial wedges h and g are truncated by an erosion surface, above which the oldest deposits are units f and e. This rupture phase, that we named R2, therefore occurred between ~10.5 ka (age of unit g) and ~9.5 ka (age of unit f).

Faults F3, F4, F5, F14, F15, F18, F19 affect units j, i, h, g, f, e and are sealed by colluvial unit d, having ceased their activity since. Given the period of more than 7000 years of no sedimentation or erosion between units e and d, they may correspond to multiple paleo-earthquakes. Their occurrence is younger than ~9.5 ka and older than ~2.3 ka. These faults were activated during a rupture phase that we called R3. This rupture phase may be distinguished by the following rupture events since a relevant erosional episode occurred between the deposit of unit e and the deposit of unit d, as suggested by the irregular geometry of the top of unit e and its sharp termination to the south. Faults related to rupture phase R3 are all truncated by this erosional episode, which predates unit d deposit.

Fault F10 on the east wall and its counterpart F11 broke during rupture phase R2. But this fault was reactivated several times after this period. On the east wall F10 offsets the fluvial unit j and limits upslope colluvial units d and c. This geometry associated with the sedimentary composition of these units strongly suggests that d and c are colluvial wedges formed during a rupture event that we named R4. The robust dating of units d to b* allows an accurate age of R4 at 2160 ± 170 cal yrs BP. The presence of two large colluvial wedges of similar ages strongly suggest the occurrence of two major earthquakes in less than 2 centuries. The multiple verticalized cobbles in the colluvial units leaning against fault F10–F11 and the deformed sedimentary structures suggest further reactivation during more recent events. This is confirmed by the small scarp (~10 cm) at surface created by a deformation affecting the soil. However, the apparent vertical offset of ~1 m of the top of unit j clearly shows that the latest event is only responsible for a limited part of the whole deformation accommodated on this fault.

A later rupture event R5 caused the opening of a 70-cm wide and 1.30-m deep fissure (unit a) outlined by the faults F6 and F7. The disorganized sedimentary structure suggests that the open-crack was filled by the

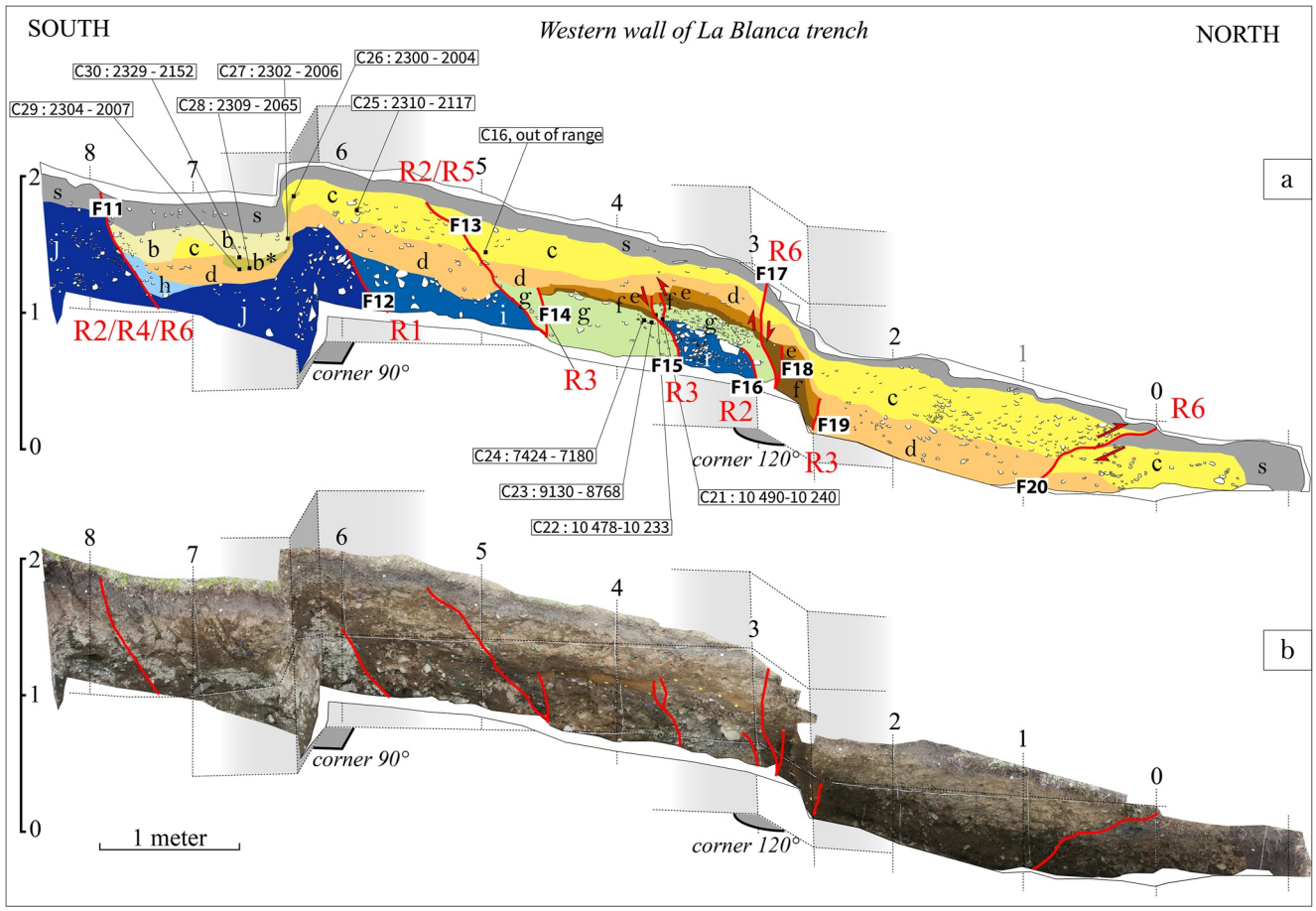

Figure 7. (a) Interpretation and (b) orthophoto mosaic of the western wall of Trench n°1. The western trench wall is not straight, the perspective of the cutting is shown with dashed line grid and angles indicated in degrees. Small black squares show the locations of radiocarbon samples, labeled by sample numbers and their corresponding calibrated radiocarbon ages (cal yrs BP). Rupture events or phases (R), associated faults (F) and fault kinematics (arrows) are marked in red. Zoom on soft sediment deformation is available in Supporting Information S1.

surrounding material at the time of the rupture. Cobbles and pebbles fell first inside the fissure, which was then entirely filled by fine-grained material. The mix of 3 charcoals in the same age range with two older charcoals buried at different depths, from 0.3 m up to 1.20 m, supports the chaotic nature of the deposit. The present soil above the fissure is undamaged and hosts horizontally oriented pebbles, clearly sealing the ruptures (Figure 6). On the western wall, this event appears to be related to fault F13 (Figure 7). The age of unit a dates rupture event R5 at 860 ± 130 cal yrs BP.

Lastly, the youngest rupture event R6 affects symmetrically both walls and is associated with multiple faults. At the bottom of the scarp, several faults with reverse component disrupt the entire section (F1, F2, F17, F20) and bury modern soil wedges. Along F1-F20 an apparent slip of ~10 cm is measured. Along the sub-vertical fault F2-F17 the offset is around 25 cm. The modern soil is clearly truncated also along the fault F10–F11, which was re-activated at this time (Figures 6 and 7). Furthermore, in trench n°2, fault A also disrupts the surface and damages the modern soil (Figure 3). These truncations in modern soil are consistent with the Riedel fractures observed in the morphology. Accordingly, the rupture event R6 might be referred to the historical earthquakes that occurred in 1949 CE and possibly also 1879 CE.

Finally, units e and f show convoluted features and flame-like structures typical of seismically induced soft-sediment deformations. These structures intrude and deform the base of unit d. Injection of pebbles along the fault F5 crosses the units e and f along a sub-horizontal clastic-sill. Given their stratigraphic position and geometry, these structures formed during an earthquake after the deposit of unit d and may therefore be associated with rupture events R5 or R6.

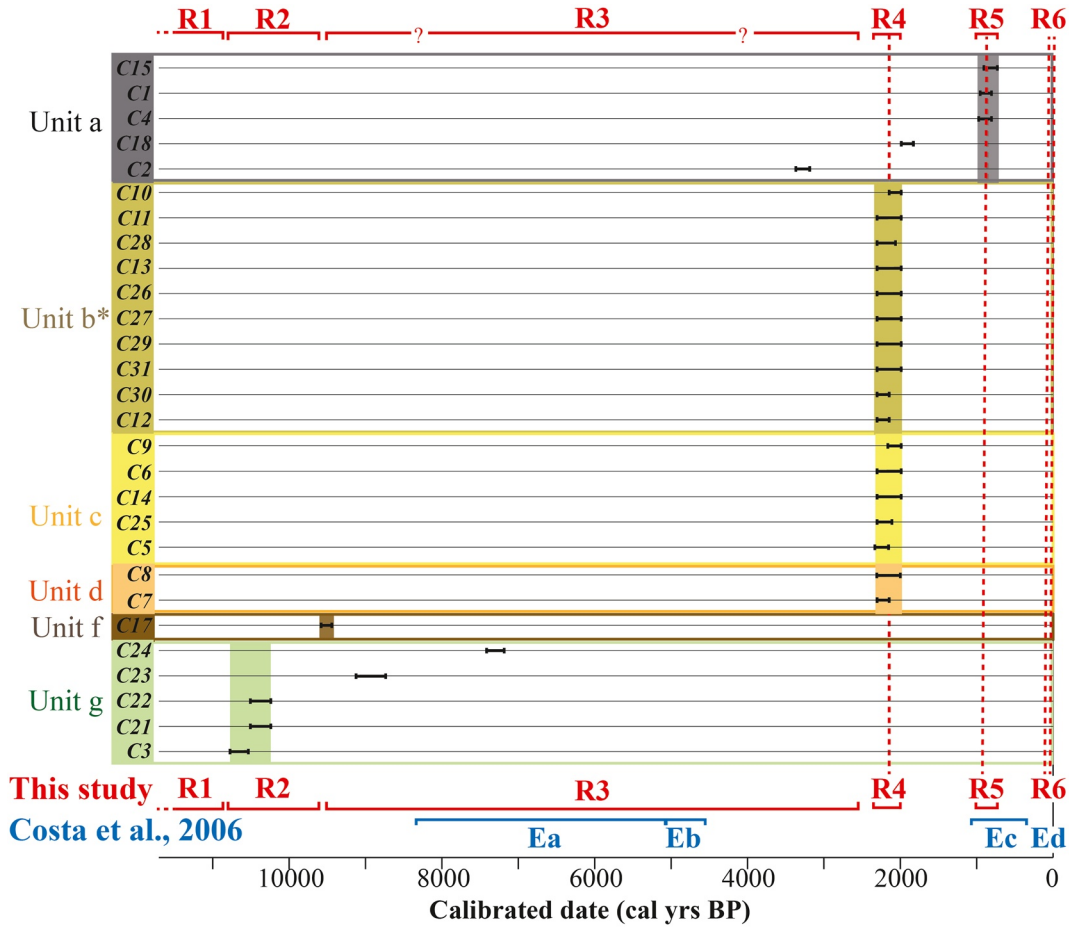

Figure 8. Calibrated ages calculated for samples collected in the trench. Age models are calculated for charcoals using OxCal v4.3.2 (Ramsey, 2009) and the Southern Hemisphere calibration curve SHCal13 (Hogg et al., 2013). Time is shown in calendar years BP (present refers to 1950). Colored zones indicate the units that contained charcoals. Ages assigned to units are discussed in the text. Observed rupture events or phases are shown with red dashed lines. Ages of ruptures determined by Costa et al. (2006) in the San Pablo Fault section are indicated in blue.

We conclude that the paleoseismic observations in La Blanca section put in evidence at least six rupture events or phases (Figures 8 and 9). The latest one corresponds to the historical earthquakes of 1949 and possibly 1879 CE, named R6. The penultimate rupture event was accurately dated at 860 ± 130 cal yrs BP (R5). The previous rupture event occurred at 2160 ± 170 cal yrs BP, and is probably associated with two paleo-earthquakes (R4). A long period without sedimentation yields poor constrains on the number and ages of the paleo-earthquakes of the previous rupture phase: at least one paleo-earthquake occurred between ~9.5 ka and ~2.3 ka (R3). The previous rupture phase is dated between ~10.5 and ~9.5 ka (R2). Finally, the oldest rupture phase recorded in our trench occurred before ~10.5 ka.

4.4. Relationships Between Micro-Topography and Faults Observed in Trenches

The micro-topography analysis of the trenches site shows four main Riedel fractures A, B, C, and D with orientation N75° to N70° (Figure 3). These Riedel fractures cross the two trenches, displaying sub-vertical dips. Fracture A is visible in Trench n°2, separating gray alluvial material of the southern block from brown colluvial material of the northern block. Fractures B, C and D are visible in Trench n°1 and correspond respectively to the faults F10/F11, F6-7/F13, and F1/F20. As previously shown, these faults disrupt the soil horizon reaching the surface and formed small scarps or elongated depressions of 10–20 cm high. It is interesting to notice that they are associated both to the latest rupture (R6) and to the penultimate one (R5). It means that their trace at surface along the scarp may last for a thousand years.

As expected, older ruptures sealed by successive colluvial deposits do not perturb the scarp topography. However, the long-term localized and distributed deformation, in spite of the dominant strike-slip kinematics, is responsible

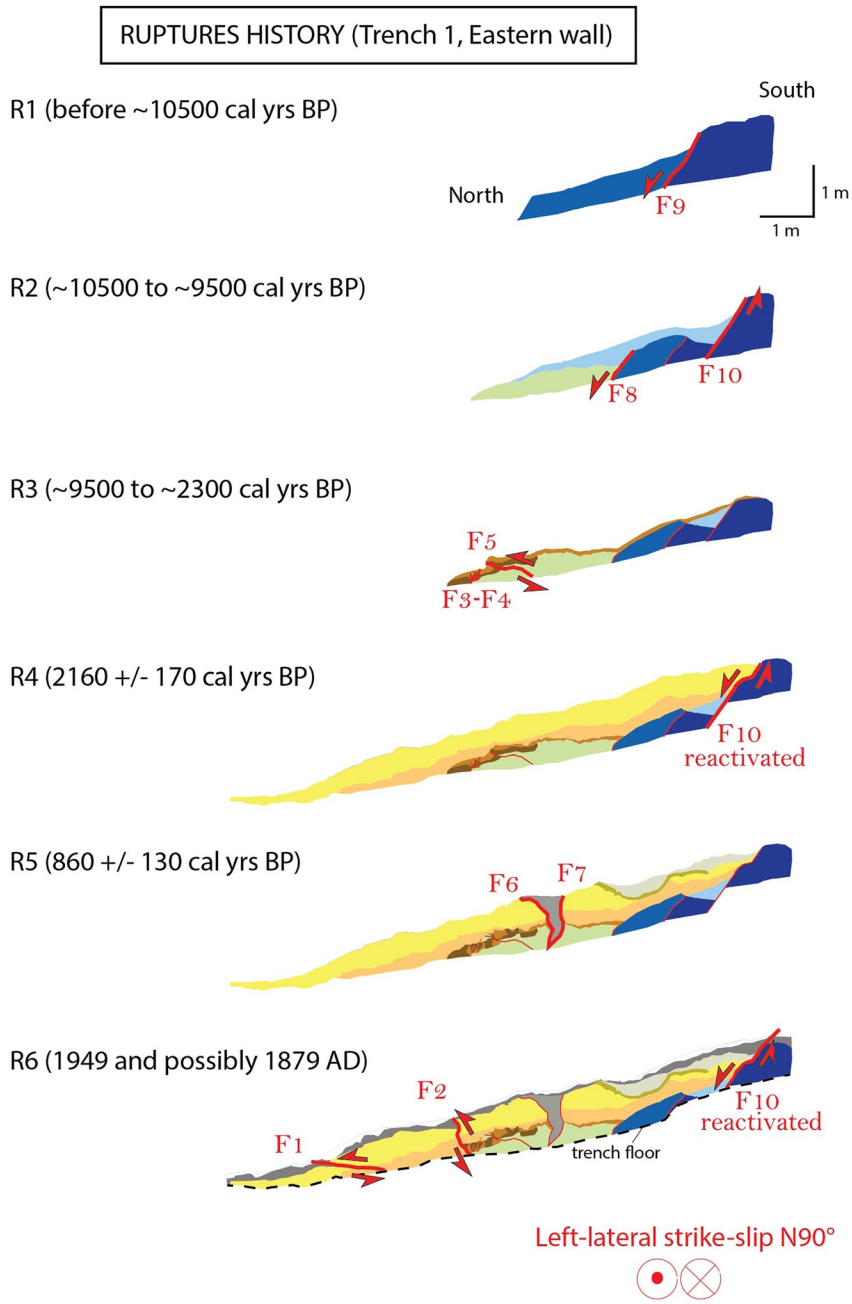

Figure 9. Palinspastic restoration of tectonic and sedimentary episodes observed in the eastern wall of Trench n°1. Bold red lines correspond to the faults activated at each rupture event or phase. The final stage (R6) was drawn using the present trench log.

for the uplift of ~10 m of the southern block. Fault branches observed in the trenches show both reverse and normal dip-slip components (Figure 3). Oblique-reverse branches are south-dipping and mostly situated in the lower part of the scarp, while oblique-normal branches are north-dipping and situated in the middle part of the scarp.

5. Discussion

5.1. Co-Seismic Versus Long-Term Fault Kinematics

In our study area, the ratio between horizontal slip (4.3–6.5 m, estimated by Roy et al. (2020)) and vertical slip (0.3–0.5 m, estimated from observed ruptures in this study) for the last earthquake is around 10. If this ratio

applies as well to the long-term we should expect that the present scarp (10 m) corresponds to a lateral slip in the order of hundred meters. The cumulated lateral offset cannot be directly estimated on this fault segment. However, the post-glacial slip was estimated a few kilometres to the west, where two abandoned glacio-fluvial valleys show left-lateral offset of respectively 115 ± 5 m of Roy et al. (2020) and 110 ± 5 m to 130 ± 10 m (Sandoval & De Pascale, 2020). Considering a similar age for the abandonment of the large glacio-fluvial terraces along the fault zone, as suggested by previous dating around 18–20 ka (Roy et al., 2020), we propose that this offset applies to our study area as well. It suggests that co-seismic and long-term ratios between lateral and vertical slip are of the same order of magnitude.

5.2. Comparison of Paleoseismological Results With Other Records

We compare our paleoseismological observations in the La Blanca trenches with the few regional records of large earthquakes along the Magallanes-Fagnano fault. We first consider the two historical earthquakes of 1879 and 1949, felt by the population and recorded by tree-rings anomalies along the fault scarp (Pedrera et al., 2014). We then attempt a correlation with paleoseismic investigations in the San Pablo section (Costa et al., 2006). We finally discuss the possible relationships with mass-wasting events observed in Lago Fagnano, 40 km to the west (Waldmann et al., 2011).

5.2.1. Historical Earthquakes Recorded by Tree-Ring Anomalies

The whole region was shaken by the 1879 and 1949 historical earthquakes. The short time-interval between these two earthquakes prevents the possibility of distinguishing ruptures associated to the former or the latter one in trenches. The rupture event that we named R6 may therefore represent 1949 and possibly 1879 earthquakes. Nevertheless, south of the Lake Udaeta and only 6-km from our trench site, Pedrera et al. (2014) analyzed tree-rings in trees located on the fault trace. Tree-rings anomalies show that several trees were tilted both in 1879 and 1949. This result strongly suggests that both earthquakes were large enough to produce ground deformation and primary surface ruptures in this zone. These data would support the hypothesis that the youngest rupture geometries observed in the trenches are resulting from both the 1879 and 1949 earthquakes. For earthquakes separated by few years or decades over the last centuries, the time resolution of tree-ring analysis is a precious tool for distinguishing undifferentiated events in trenches.

5.2.2. Correlation With the Trench in the San Pablo Fault Section

Costa et al. (2006) identified four seismic events in a trench excavated on the MFF 24 km west of our study site. This trench was dug through a secondary branch of the fault, which means that it might not have recorded all the major earthquakes that ruptured this fault section. There are no pictures available of the trench walls, thus we have to deal with the interpreted logs and authors hypothesis. Moreover, dating of the events is based on a few radiocarbon samples, which do not allow to determine an accurate recurrence interval. For comparison, we recalibrated ages obtained by Costa et al. (2006) in cal yrs BP according the calibration curve (SHCAL13). To avoid confusion in the rupture numbering, we label the events from Costa et al. (2006) Ed to Ea from the youngest to the oldest (Figure 8).

The youngest event ruptures the modern soil, as in our trench, and therefore corresponds to the historical earthquakes of 1949 and possibly of 1879. This event also offset local anthropogenic features like fences (Costa et al., 2006) and a wooden bridge (Roy et al., 2020), confirming that deformation affected the surface at this site, at least during the 1949 event. As in our study, it is not possible to distinguish in the trench if one or two earthquakes are recorded. This event, that we name Ed, corresponds to our R6 rupture event.

The penultimate event is bracketed by Costa et al. (2006) using a unit characterized by sharp thickness variation across the fault as being a pre-event marker, and the successive unit with no deformation at its base as a post-event marker. The disrupted unit is dated from 1059–922 cal yrs BP to 781–666 cal yrs BP, while the undeformed unit is dated at 537–326 cal yrs BP. Tectonic deformation occurred between ~1000 and ~400 cal yrs BP. This event (Ec) is therefore compatible with rupture event R5 found at La Blanca section.

Costa et al. (2006) recognize two older events that occurred between 5277 and 4571 cal yrs BP and between 8343 and 5051 cal yrs BP, even though the relationships between stratigraphy and ruptures are not straightforward on both walls. First, this means that the pre-penultimate earthquake of La Blanca section (~2.2 ka R4 paleo-earthquake) was not observed here. Second, these two events occurred in a period of no sedimentation in

La Blanca trench. We put in evidence at least one earthquake between ~9.5 ka and ~2.3 ka (rupture phase R3), which may correspond to one of them, but the uncertainty on the ages are too high to speculate on that.

More generally, ruptures on the primary fault trace in the La Blanca trench are well expressed where they are still preserved. On the other hand, at this site, long hiatus in the sedimentation process are an impediment for having a complete history of rupture events. The opposite is true on the secondary fault trace in San Pablo section (Costa et al., 2006), where the paleoseismic signal is more difficult to decipher or absent for some earthquakes, but the more continuous sedimentation allows recording tectonic deformation through a more continuous period. The integration of La Blanca and San Pablo trenches allows to precisely reconstruct the past 2000 years history of the MFF, taking advantage of the complementary record of these two sites.

5.2.3. Relationships With Mass-Wasting Events in Lago Fagnano

The high-resolution seismic lines analyzed by Waldmann et al. (2011) image several Holocene mass-wasting events that occurred in the eastern sub-basin of Lago Fagnano, ~40 km west of La Blanca trenches. Waldmann et al. (2011) argue that these events resulted from seismic activity. They consider that the subduction of the Antarctic plate beneath southern Chile is too far from the lake, and assume that the observed mass-wasting deposits were triggered by major earthquakes affecting the Magallanes-Fagnano Fault zone.

Ages of mass-wasting events in the lake are constrained by eight radiocarbon ages obtained in four stratigraphy-correlated distinct cores, and by a 7.6 kyrs-old tephra coming from the Hudson volcano observed in the four cores. To assess an age to the different mass-wasting events, Waldmann et al. (2011) calculated the average background sedimentation rate (i.e., the sedimentation rate obtained removing mass-flow deposits) that prevailed since the deposition of the tephra found in one of the cores (core LF06-PC16). They supposed that this sedimentation rate remained constant, even though substantial rate changes may have occurred resulting from variable climatic conditions during the Holocene (Coronato et al., 2011). Considering the thickness of the sediments that cover the mass-wasting deposits, Waldmann et al. (2011) estimated their ages and noted that radiocarbon ages are systematically older than those that are extrapolated from the calculated background sedimentation rate based only on the tephra age. They conclude that sampled charcoals may be reworked and that radiocarbon data may only provide maximum deposition ages. Then, it is not possible to date precisely the mass-wasting events that occurred in the lake. Obtained ages would have been different considering a constant sedimentation rate in another of the four cores, or considering that radiocarbon ages indicate the true deposition age of the layer in which they were obtained (Waldmann, 2008).

Despite the uncertainty about the age of each mass-flow event, Waldmann et al. (2011) recognize 19 major events that occurred in the last 11.3 kyrs, which gives an average recurrence interval of ~630 years. They also note that the interval between two successive events is very irregular. It is quite common to have pairs of events within 1 or 2 centuries, followed by larger quiescence periods comprised between 800 and 1100 years. Mass-flow events separated by short time intervals may possibly result from earthquakes that ruptured different portions of the fault, meaning that the average recurrence interval between two major earthquakes in the same sector of the fault may be larger than the 630 years value (Waldmann et al., 2011).

In our study, the average recurrence interval that separates well-dated events over the last two thousand years is 1080 ± 150 years. For repeated earthquakes of similar co-seismic slip (4.3–6.5 m) as the 1949 event, this interval would yield a long-term lateral slip rate of ~6 mm/yr. This extrapolated fault slip rate is compatible both with the known geodetic and geomorphic slip rates of 6–7 mm/yr (Mendoza et al., 2015; Roy et al., 2020; Sandoval & De Pascale, 2020; Smalley et al., 2003).

However, despite the millennial average recurrence interval, the latest event R6 is likely constituted by two earthquakes that occurred in less than a century. This pattern is very similar to what observed in mass-wasting deposits in Lago Fagnano, where in spite of the inaccurate chronology, Waldmann et al. (2011) show that there are couple of events occurring close in time separated by longer interevent intervals. It is interesting to note that we obtain a similar conclusion from our trenches for some events, in particular 1949 with possibly 1879 (R6) and probably around 2160 cal yrs BP (R4). We have to understand whether these "paired earthquakes" are of similar magnitude, meaning that fault behavior is far to be based on regular seismic cycles, or if on the contrary their sizes are significantly different, implying an apparent over-representation of the seismicity both in trenches and in lake sediments.

6. Conclusions

The paleoseismological results from La Blanca section put in evidence at least six major rupture events or phases along the Eastern portion of the Magallanes-Fagnano Fault. Primary surface ruptures show a dominant left-lateral strike-slip kinematics, compatible with the Late Quaternary cumulated topography. We reconstructed a surface faulting history for this portion of the Magallanes-Fagnano Fault over the last two thousand years. Over this period, three rupture events are dated at 1949 CE (and possibly 1879), 860 ± 130 cal yrs BP, and 2160 ± 170 cal yrs BP. The two latest events are coeval with those found in another trench study on the MFF (Costa et al., 2006), and our results allow refining the age of the penultimate one. Three older rupture phases are recorded in the trench with a less accurate chronology until ∼10,500 years ago.

Our paleoseismic results are characterized by recurrence pattern similar to that observed for mass-wasting deposits in Lago Fagnano (Waldmann et al., 2011). Mass-wasting events suggest the occurrence of "paired earthquakes" close in time separated by longer interevent intervals. In parallel, trench analysis revealed that large earthquakes may follow one another in less than 1 or 2 centuries, as observed for the events of 1949 and 1879, and possibly for two paleo-earthquakes around 2160 cal yrs BP. This seismic pattern may be due to the rupture of different neighbor sections of the fault or to different earthquake sizes, even though these scenarios should be verified by paleoseismic data at different sites along the fault.

If we consider repeated earthquakes of same co-seismic slip as the 1949 earthquake and the average recurrence intervals of ∼1000 years determined for the three latest rupture events, it would yield a long-term lateral slip rate of ∼6 mm/yr. This extrapolated fault slip rate is in agreement with both the known geodetic and geomorphic slip rates along the MFF.

Data Availability Statement

Raw ages of 28 radiocarbon samples in the paleoseismological trench n°1 across the Magallanes-Fagnano Fault are registered online with the International Geo Sample Numbers (IGSN). Samples are registered at System for Earth Sample Registration (SESAR) available at http://geosamples.org/. Samples metadata are available in the repository Sample Type "Terrestrial Section." They can be found by setting in the search box "IGSN begins with: IEROY." The IGSN numbers are indicated in Table 1 and are the following: IEROY0001, IEROY0002, IEROY0003, IEROY0004, IEROY0005, IEROY0006, IEROY0007, IEROY0008, IEROY0009, IEROY000A, IEROY000B, IEROY000C, IEROY000D, IEROY000E, IEROY000F, IEROY000G, IEROY000H, IEROY000I, IEROY000J, IEROY000K, IEROY000L, IEROY000M, IEROY000N, IEROY000O, IEROY000P, IEROY000Q, IEROY000R, IEROY000S.

Acknowledgments
This work is part of the Ph.D. thesis of Sandrine Roy funded by the French Ministry of Higher Education and Research. We acknowledge financial support by Labex@OSUG2020, Syster (INSU), Mission pour les Initiatives Transverses Interdisciplinaires (MITI), and PICS programs. This work was supported by public funds received in the framework of GEOSUD, a project (ANR-10-EQPX-20) of the program "Investissements d'Avenir" managed by the French National Research Agency. We would like to kindly acknowledge Cristian Maure and Marina Bauducco from Ushuaia for their hospitality and direct support in the field. This research is part of a new bilateral scientific cooperation project between Universidad de Tierra del Fuego (Ushuaïa) and the University Savoie Mont-Blanc (ISTerre). We are grateful to Mónica P. Escayola and Dr. Daniel A. Fernández (CONICET, Instituto de Ciencias Polares, Ambiente y Recursos Naturales-ICPA, Universidad Nacional de Tierra del Fuego) for the discussions and the logistical help in Tierra del Fuego. We warmly thank Mr. Fabien Massot for his precious and unswerving administrative support. We greatly acknowledge M. Ghiglione, D. Pantosti, and C. Costa for their constructive and very detailed reviews that helped us to considerably improve the paper.

References

Adaros, R. E., Wiens, D. A., Vera, E. E., & Shore, P. J. (1999). Seismicity and tectonics of southern Patagonia from a local deployment of seismographs: Preliminary results. In *AEO, 80, Fall Meeting, Supplement Abstract A52A-05*.

Blair, T. C., & McPherson, J. G. (1999). Grain-size and textural classification of coarse sedimentary particles. *Journal of Sedimentary Research*, *69*(1), 6–19. https://doi.org/10.2110/jsr.69.6

Bridges, E. L. (1948). *The uttermost part of the Earth*. Hodder & Stoughton.

Bridges, T., & Canclini, A. (2001). *Los indios del último confín: Sus escritos para la South American Missionary Society*. Zagier & Urruty.

Brüggen, J. (1943). Contribución a la geología sísmica de Chile. *Revista Chilena de Historia y Geografía*, *103*, 108–174.

Bustos, J. (1931). Estudio sismológico de Chile con los temblores y terremotos producidos en los últimos cuatro siglos. *Anales de la Universidad de Chile*, *1*, 59–91.

Castano, J. C. (1977). *Zonificación sísmica de la República Argentina* (p. 40). Publicación Técnica N° 5.

Cisternas, A., & Vera, E. (2008). Sismos históricos y recientes en Magallanes. *Magallania (Punta Arenas)*, *36*, 43–51. https://doi.org/10.4067/S0718-22442008000100004

Coronato, A., Fanning, P., Salemme, M., Oría, J., Pickard, J., & Ponce, J. F. (2011). Aeolian sequence and the archaeological record in the fuegian steppe, Argentina. *Quaternary International*, *245*(1), 122–135. https://doi.org/10.1016/j.quaint.2011.02.042

Costa, C. H., Smalley, R., Velasco, M. S., Schwart, D. P., Ellis, M., & Ahumada, E. A. (2006). Paleoseismic observations of an onshore transform boundary: The Magallanes-Fagnano fault, Tierra del Fuego, Argentina. *Revista de la Asociación Geológica Argentina*, *61*(4), 647–657.

Dublé Almeida, D. (1938). Diario de viaje al río Santa Cruz, Patagonia. *Revista Chilena de Historia y Geografía*, *93*, 254–279.

Eagles, G., & Jokat, W. (2014). Tectonic reconstructions for paleobathymetry in Drake Passage. *Tectonophysics*, *611*, 28–50. https://doi.org/10.1016/j.tecto.2013.11.021

Elliott, D. (1983). The construction of balanced cross-sections. *Journal of Structural Geology*, *5*(2), 101. https://doi.org/10.1016/0191-8141(83)90035-4

Esteban, F. D., Tassone, A., Lodolo, E., Menichetti, M., Lippai, H., Waldmann, N., et al. (2014). Basement geometry and sediment thickness of Lago Fagnano (Tierra del Fuego). *Andean Geology*, *41*(2), 293–313. https://doi.org/10.5027/andgeoV41n2-a02

Febrer, J. M., Plasencia, M. P., & Sabbione, N. C. (2000). Local and regional seismicity from Ushuaia broadband station observations (Tierra del Fuego). *Terra Antartica*, *8*, 35–40.
Ghiglione, M. C. (2002). Diques clásticos asociados a deformación transcurrente en depósitos sinorogénicos del Mioceno inferior de la Cuenca Austral. *Revista de la Asociación Geológica Argentina*, *57*, 103–118.
Ghiglione, M. C., & Ramos, V. A. (2005). Progression of deformation and sedimentation in the southernmost Andes. *Tectonophysics*, *405*(1–4), 25–46. https://doi.org/10.1016/j.tecto.2005.05.004
Hogg, A. G., Hua, Q., Blackwell, P. G., Niu, M., Buck, C. E., Guilderson, T. P., et al. (2013). SHCal13 Southern Hemisphere calibration, 0–50,000 years cal BP. *Radiocarbon*, *55*(4), 1889–1903. https://doi.org/10.2458/azu_js_rc.55.16783
INPRES. (2021). Terremotos históricos ocurridos en la República Argentina. Retrieved from http://contenidos.inpres.gob.ar/sismologia/historicos
Isla, F. I., & Bujalesky, G. (2004). El maremoto de los Yaganes. *Nexos, UNMDP, Mar del Plata*, *19*, 29–33.
Jaschek, E. U., Sabbione, N. C., & Sierra, P. J. (1982). *Reubicación de sismos localizados en territorio Argentino, 1920–1963*. Observatorio Astronomico de la Universidad nacional de la Plata.
Klepeis, K. A. (1994). The Magallanes and Deseado fault zones: Major segments of the South American-Scotia transform plate boundary in southernmost South America, Tierra del Fuego. *Journal of Geophysical Research: Solid Earth*, *99*(B11), 22001–22014. https://doi.org/10.1029/94JB01749
Lodolo, E., Menichetti, M., Bartole, R., Ben-Avraham, Z., Tassone, A., & Lippai, H. (2003). Magallanes-Fagnano continental transform fault (Tierra del Fuego, southernmost South America). *Tectonics*, *22*(6), 15–26. https://doi.org/10.1029/2003TC001500
Lomnitz, C. (1970). Major earthquakes and tsunamis in Chile during the period 1535 to 1955. *Geologische Rundschau*, *59*(3), 938–960. https://doi.org/10.1007/BF02042278
Martinic, M. B. (1988). El gran temblor de tierra de 1879 en la Patagonia Austral. *Revista Patagónica*, 30–31.
Martinic, M. B. (2008). Registro Histórico de Antecedentes Volcánicos y Sísmicos en la Patagonia Austral y la Tierra del Fuego. *Magallania*, *36*(2), 5–18. https://doi.org/10.4067/S0718-22442008000200001
Massone, M. (2004). *Los cazadores después del hielo* (p. 173). Centro de investigación D. Barros Arana.
Mc Calpin, J. (1996). *Paleoseismology*. *International Geophysics Series* (Vol. 62, p. 588). Academic Press.
McCalpin, J. P., & Nelson, A. R. (1996). Chapter 1 Introduction to paleoseismology. In J. P. McCalpin (Ed.), *International Geophysics* (Vol. 62, pp. 1–32). https://doi.org/10.1016/S0074-6142(96)80068-4
Mendoza, L., Richter, A., Fritsche, M., Hormaechea, J. L., Perdomo, R., & Dietrich, R. (2015). Block modeling of crustal deformation in Tierra del Fuego from GNSS velocities. *Tectonophysics*, *651–652*, 58–65. https://doi.org/10.1016/j.tecto.2015.03.013
Miotti, L., & Salemme, M. (2004). Poblamiento, movilidad y territorios entre las sociedades cazadoras-recolectoras de Patagonia. *Complutum*, *15*, 177–206. https://doi.org/10.1016/S1571-0866(07)10022-1
Montessus de Ballore, F. (1912). Geografía sísmica de Chile. *Revista Chilena de Historia y Geografía*, *7*, 178–195.
Obermeier, S. F. (1996). Use of liquefaction-induced features for paleoseismic analysis—An overview of how seismic liquefaction features can be distinguished from other features and how their regional distribution and properties of source sediment can be used to infer the location and strength of Holocene paleo-earthquakes. *Engineering Geology*, *44*(1–4), 1–76. https://doi.org/10.1016/S0013-7952(96)00040-3
Onorato, M. R. (2018). *Influencia de la neotectónica y la glaciotectónica en geoformas y depósitos sedimentarios glacigénicos: Herramientas para el estudio y análisis de los procesos glaciotectónicos y la paleosismicidad en la Isla Grande de Tierra del Fuego* (Ph.D) (p. 242). Universidad Nacional de San Juan.
Onorato, M. R., Coronato, A., Perucca, L., Rabassa, J., & López, R. (2017). Morpho-bathymetry and surficial morphology of Udaeta Lake, along the Magallanes-Fagnano fault system, Tierra del Fuego, Argentina. *Journal of South American Earth Sciences*, *76*, 1–10. https://doi.org/10.1016/j.jsames.2017.02.001
Onorato, M. R., Perucca, L. P., Coronato, A., Prezzi, C., Blanc, P. A., Lopez, R., & Magneres, I. (2021). Morphotectonic characterization along the eastern portion of the main trace of Magallanes-Fagnano Fault System in Tierra del Fuego, Argentina. *Journal of South American Earth Sciences*, *112*, 103550. https://doi.org/10.1016/j.jsames.2021.103550
Palacios, R. A. (2013). Notas históricas del primer sismo registrado en la ciudad de Punta Arenas y en la región de Magallanes en Febrero de 1879. *Magallania (Punta Arenas)*, *41*(2), 215–220. https://doi.org/10.4067/S0718-22442013000200012
Pedrera, A., Galindo-Zaldívar, J., Ruiz-Constán, A., Bohoyo, F., Torres-Carbonell, P., Ruano, P., et al. (2014). The last major earthquakes along the Magallanes–Fagnano fault system recorded by disturbed trees (Tierra del Fuego, South America). *Terra Nova*, *26*(6), 448–453. https://doi.org/10.1111/ter.12119
Pelayo, A. M., & Wiens, D. A. (1989). Seismotectonics and relative plate motions in the Scotia Sea region. *Journal of Geophysical Research*, *94*(B6), 7293–7320. https://doi.org/10.1029/JB094iB06p07293
Perucca, L., Alvarado, P., & Saez, M. (2016). Neotectonics and seismicity in southern Patagonia. *Geological Journal*, *51*(4), 545–559. https://doi.org/10.1016/S1571-0866(07)10005-1
Ramsey, C. B. (2009). Bayesian analysis of radiocarbon dates. *Radiocarbon*, *51*(1), 337–360. https://doi.org/10.1017/S0033822200033865
Ramsey, C. B. (2017). Methods for summarizing radiocarbon datasets. *Radiocarbon*, *59*(6), 1809–1833. https://doi.org/10.1017/RDC.2017.108
Roy, S. (2020). *Tierra del Fuego: Interaction between tectonics and climate in the southern end of America* (Ph.D) (p. 278). Université de Savoie Mont Blanc.
Roy, S., Vassallo, R., Martinod, J., Ghiglione, M. C., Sue, C., & Allemand, P. (2020). Co-seismic deformation and post-glacial slip rate along the Magallanes-Fagnano fault, Tierra Del Fuego, Argentina. *Terra Nova*, *32*, 1–10. https://doi.org/10.1111/ter.12430
Roy, S., Vassallo, R., Martinod, J., & Sue, C. (2022). Raw ages of 28 radiocarbon samples in paleoseismological trench n°1 across the Magallanes-Fagnano Fault, Tierra del Fuego, Argentina [Dataset]. SESAR. http://geosamples.org/
Salemme, M. C., & Miotti, L. L. (2008). Archeological hunter-gatherer landscapes since the latest Pleistocene in Fuego-Patagonia. *Developments in Quaternary Sciences*, *11*, 437–483. https://doi.org/10.1016/S1571-0866(07)10022-1
Sandoval, F. B., & De Pascale, G. P. (2020). Slip rates along the narrow Magallanes fault System, Tierra del Fuego Region, Patagonia. *Scientific Reports*, *10*, 1–13. https://doi.org/10.1038/s41598-020-64750-6
Serrano, R. (1880). Diario de la excursión a la isla grande de la Tierra del Fuego durante los meses de enero y febrero de 1879. *Anuario Hidrográfico de la Marina de Chile*, *VI*, 151–204.
Sieh, K. E. (1981). A review of geological evidence for recurrence times of large earthquakes. *Earthquake Prediction: An International Review*, *4*, 181–207. https://doi.org/10.1029/ME004p0181
Simpson, J., & Chaigneau, F. (1880). Diario llevado por los tenientes Simpson y Chaigneau: En Latorre, Exploracion de las aguas de Skyring o del Despejo. *Anuario Hidrográfico de la Marina de Chile*, *VI*, 73–96.

Smalley, R., Kendrick, E., Bevis, M. G., Dalziel, I. W. D., Taylor, F., Lauría, E., et al. (2003). Geodetic determination of relative plate motion and crustal deformation across the Scotia-South America plate boundary in eastern Tierra del Fuego. *Geochemistry, Geophysics, Geosystems*, *4*(9), 1070. https://doi.org/10.1029/2002GC000446

Tassone, A., Lippai, H., Lodolo, E., Menichetti, M., Comba, A., Hormaechea, J. L., & Vilas, J. F. (2005). A geological and geophysical crustal section across the Magallanes–Fagnano fault in Tierra del Fuego. *Journal of South American Earth Sciences*, *19*(1), 99–109. https://doi.org/10.1016/j.jsames.2004.12.003

Tassone, A., Lodolo, E., Menichetti, M., Yagupsky, D. L., Caffau, M., & Vilas, J. F. A. (2008). Seismostratigraphic and structural setting of the Malvinas Basin and its southern margin (Tierra del Fuego Atlantic offshore). *Geológica Acta*, *6*, 55–67.

Torres-Carbonell, P. J., Dimieri, L. V., Olivero, E. B., Bohoyo, F., & Galindo-Zaldívar, J. (2014). Structure and tectonic evolution of the Fuegian Andes (southernmost South America) in the framework of the Scotia Arc development. *Global and Planetary Change*, *123*, 174–188. https://doi.org/10.1016/j.gloplacha.2014.07.019

Torres-Carbonell, P. J., Olivero, E. B., & Dimieri, L. V. (2008). Control en la magnitud de desplazamiento de rumbo del Sistema Transformante Fagnano, Tierra del Fuego. *Revista Geológica de Chile*, *35*(1), 63–77. https://doi.org/10.5027/andgeoV35n1-a03

U.S. Geological Survey. (2021). Earthquake maps and statistics. Retrieved from https://www.usgs.gov/programs/earthquake-hazards/lists-maps-and-statistics

Waldmann, N. (2008). *Late Quaternary environmental changes in Lago Fagnano, Tierra del Fuego (54°S): Reconstructing sedimentary processes, natural hazards and paleoclimate* (Ph.D) (p. 154). Université de Genève.

Waldmann, N., Anselmetti, F. S., Ariztegui, D., James, A., Austin, J., Pirouz, M., et al. (2011). Holocene mass-wasting events in Lago Fagnano, Tierra del Fuego (54°S): Implications for paleoseismicity of the Magallanes-Fagnano transform fault. *Basin Research*, *23*(2), 171–190. https://doi.org/10.1111/j.1365-2117.2010.00489.x

Wallace, R. E. (1981). Active faults, paleoseismology, and earthquake hazards in the western United States. *Earthquake prediction: an international review*, *4*, 209–216. https://doi.org/10.1029/ME004p0209

Winslow, M. A. (1982). The structural evolution of the Magallanes Basin and neotectonics in the southernmost Andes. *Antarctic Geoscience*, *4*, 143–154.